CHALMERS
UNIVERSITY OF TECHNOLOGY

Sustainable Heat Generation in Flow from a Molecular Solar Thermal Energy Storage System

Downloaded from: https://research.chalmers.se, 2026-01-27 12:22 UTC

Citation for the original published paper (version of record):
Magson, L., Jonsson Maggiolo, D., Sasic Kalagasidis, A. et al (2025). Sustainable Heat Generation in Flow from a Molecular Solar Thermal Energy Storage System. Advanced Energy and Sustainability Research, 6(1). http://dx.doi.org/10.1002/aesr.202400230

N.B. When citing this work, cite the original published paper.

research.chalmers.se offers the possibility of retrieving research publications produced at Chalmers University of Technology. It covers all kind of research output: articles, dissertations, conference papers, reports etc. since 2004. research.chalmers.se is administrated and maintained by Chalmers Library

(article starts on next page)

ADVANCED ENERGY & SUSTAINABILITY RESEARCH
www.advenergysustres.com

Sustainable Heat Generation in Flow from a Molecular Solar Thermal Energy Storage System

Lucien Magson, Dario Maggiolo, Angela Sasic Kalagasidis, Stefan Henninger, Gunther Munz, Markus Knäbbeler-Buß, Helen Hölzel, Kasper Moth-Poulsen, Ignacio Funes-Ardoiz,* and Diego Sampedro**

As the global deployment of renewable technologies accelerate, finding efficient ways to store energy will aid in responding to shifting energy demands. A prospective option not only in harvesting solar energy but also in emission-free heating is MOlecular Solar Thermal (MOST) energy storage. A central part of MOST applications is to develop methods to release the stored energy. Herein, the Quadricyclane (QC)-to-Norbornadiene catalyzed back reaction is explored in a specially designed packed-bed reactor. Four distinctly sized and purposely synthesized platinum on activated carbon catalysts are studied to trigger the heat release from the energy-dense QC isomer. The catalysts are fully characterized using a variety of structural, surface, and spectroscopic techniques. Parameters to optimize catalytic conversion and heat release in flow conditions are explored including particle size and packing behavior, flow rates, and molecular residence times. Moreover, using CO pulse chemisorption technique, site time yield values and a turnover number are reported. Complementary to the flow reactions, computational fluid dynamic simulations applying lattice Boltzmann methods to two catalytic packed beds of different size ranges are done to evaluate fluid-dynamic behavior within the reactor bed to ascertain the ideal particle size and packing density for catalysis in MOST applications.

1. Introduction

In 2022, extreme weather has caused an additional demand on cooling and heating technologies, pushing up global emissions by ≈60 Mt CO_2, accounting for one-fifth of the total global increase in CO_2 emissions.[1] Two-thirds of the increase in CO_2 emissions came from additional cooling needs, where the remaining third originated from heating needs. Hence due to the increasing frequency of climate events like heatwaves, floods, droughts, and forest fires,[2] CO_2 emissions originating from heating and cooling needs are expected to continuously rise to maintain habitable living quarters. Heat pumps have become the primary technology for space heating, meeting 10% of global needs in buildings.[3] Alternative technologies with a lower carbon footprint need to be developed to maintain a more habitable indoor climate. In that regard, MOST systems utilize solar power to induce energy storage

L. Magson, I. Funes-Ardoiz, D. Sampedro
Departamento de Química
Instituto de Investigación Química de la Universidad de La Rioja
Universidad de la Rioja
C/Madre de Dios 53, 26006 Logroño, La Rioja, Spain
E-mail: Ignacio.funesa@unirioja.es; Diego.sampedro@unirioja.es

D. Maggiolo
Department of Mechanics and Maritime Sciences
Chalmers University of Technology
SE-412 96 Gothenburg, Sweden

A. S. Kalagasidis
Department of Architecture and Civil Engineering
Chalmers University of Technology
SE-412 96 Gothenburg, Sweden

The ORCID identification number(s) for the author(s) of this article can be found under https://doi.org/10.1002/aesr.202400230.

© 2024 The Author(s). Advanced Energy and Sustainability Research published by Wiley-VCH GmbH. This is an open access article under the terms of the Creative Commons Attribution License, which permits use, distribution and reproduction in any medium, provided the original work is properly cited.

DOI: 10.1002/aesr.202400230

S. Henninger, G. Munz
Heating and Cooling Technologies
Fraunhofer Institute for Solar Energy Systems (ISE)
Heidenhofstrase 2, 79110 Freiburg, Germany

M. Knäbbeler-Buß
Hydrogen Technologies and Electrical Energy Storage
Fraunhofer Institute for Solar Energy Systems (ISE)
Heidenhofstrase 2, 79110 Freiburg, Germany
E-mail: Markus.knaebbeler-buss@ise.fraunhofer.de

H. Hölzel, K. Moth-Poulsen
Department of Chemistry and Chemical Engineering
Chalmers University of Technology
SE-412 96 Gothenburg, Sweden

H. Hölzel, K. Moth-Poulsen
Department of Chemical Engineering
Universitat Politècnica de Catalunya
EEBE
Eduard Maristany 10-14, 08019 Barcelona, Spain

© 2024 The Author(s). Advanced Energy and Sustainability Research published by Wiley-VCH GmbH

through chemical isomerization in a molecular photoswitch. The resulting photoswitch can store chemical energy within their strained bonds and release it as latent heat or heat "on-demand," following the scheme shown in **Figure 1**. Their storage capabilities vary in energy density and reduce over time, especially at higher temperatures, in which half-lives at ambient temperature are reported. The ability to execute multiple charging and discharging cycles of solar energy capture and thermal release has possible applications in domestic heating, thermoregulated fabrics, legionella thermal disinfection, and industrial steam production.[4–7]

However, considerations need to be made to fit a MOlecular Solar Thermal (MOST) photoswitch with a certain application. For example, the demand for high output temperatures is primarily dependent on the specific energy density of the MOST molecule, ranging up to 0.927 MJ kg^{-1},[8] the solar energy capture efficiency of the photoactive stable isomer, and the kinetic stability of the metastable isomer.[9] Considering energy consumption is user dependent, tending to progressively use more energy on colder nights, MOST devices present a potential solution to mitigate the time shift between energy supply and demand. Despite significant research into developing the photochemical and storage properties of the MOST couple,[9,10] the heat release from the metastable isomer in practical devices has been far less explored, especially under continuous operation. Herein, we investigate the flow chemistry of MOST systems which will impart important insights into the feasibility of larger-scale thermal applications. In this investigation, the norbornadiene (NBD)-Quadricyclane (QC) photoswitch system 1 is selected comprising a MOST system with promising properties such as a moderately high photoswitching quantum yield of 61%, a high energy density of 0.40 MJ kg^{-1}, a long half life of 30 days at room temperature, a high solubility in toluene of 1.52 M, and a large production scalability (**Figure 2**A).[7,11,12] To examine the heat release reaction, we constructed a fixed-bed reactor in glass form (See in Figure S16, Supporting information) with an additional jacketed glass tubing in which the void between the two cylindrical glass cylinders can be evacuated to minimize convective heat losses.[13] The system was designed to accommodate a packed bed of catalyst particles and to record the temperature and conversion changes in a well-isolated environment (see Figure 2B).

Various catalytic packed beds were investigated for the back reaction whereby the packed bed changes predominantly according to their particle size and packing behavior instead of the chemical design and species present in the catalyst. In this way, details on the variation in catalytic conversion and heat release are investigated toward the practical application of heterogeneous catalytic MOST flow reactors. The aim of this investigation is to find the ideal particle size and packing density to achieve the highest catalytic conversion possible and to maximize the thermal output from the QC photoswitch. A drawback of liquid-based MOST systems is that the energy density of the photoswitch is immediately reduced upon dilution by a solvent; thus, to achieve a measurable temperature change in the packed-bed reactor, NBD/QC solutions need to reach high concentrations. The energy release of different concentrated solutions of this NBD/QC photoswitch in toluene media placed in a vacuum chamber (up to 10^{-5} mbar) was reported whereby at 0.10 M concentration, a temperature change of 6 °C was generated.[7] Using 0.10 M solutions of NBD which are photoirradiated and flow through the packed-bed reactor will still result in evident temperature changes. For this practically usable heat release device, high-vacuum conditions (10^{-5} mbar) are not attainable, in which thermal losses are expected probably lowering the maximum heat release from 6 °C. Although, differences in catalytic conversion and temperature should still be observed between runs wherein the optimal parameters such as particle size, packing behavior, flow rate, and residence time can be determined.

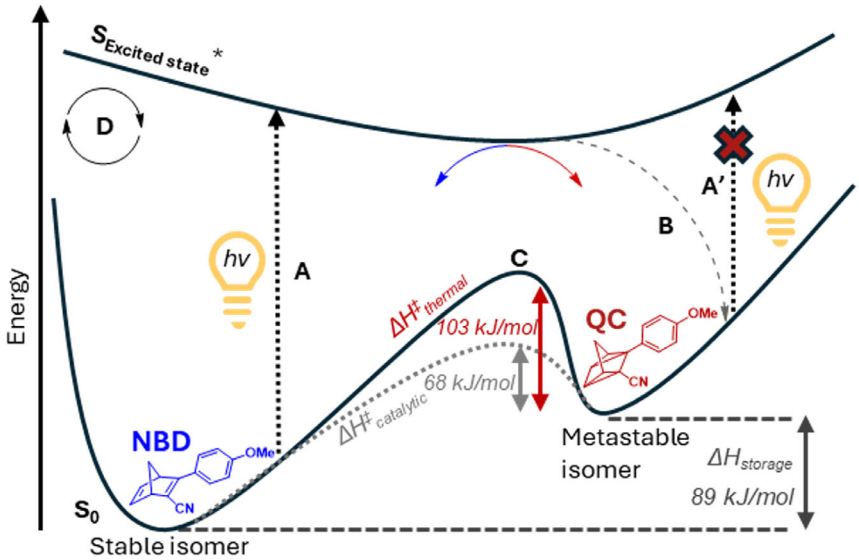

Figure 1. Scheme of the state-of-the-art NBD/QC MOST photoswitch. A represents the excitation of the stable isomer NBD upon photon absorption, A represents the undesired competitive photoexcitation of QC, C represents the thermal and catalytic barriers impeding the back reaction to the starting stable isomer, D represents the needed cyclic nature of the MOST process.

© 2024 The Author(s). Advanced Energy and Sustainability Research published by Wiley-VCH GmbH

26999412, 2025, 1, Downloaded from https://onlinelibrary.wiley.com/doi/10.1002/aesr.202400230 by Chalmers University Of Technology, Wiley Online Library on [30/01/2025]. See the Terms and Conditions (https://onlinelibrary.wiley.com/terms-and-conditions) on Wiley Online Library for rules of use; OA articles are governed by the applicable Creative Commons License

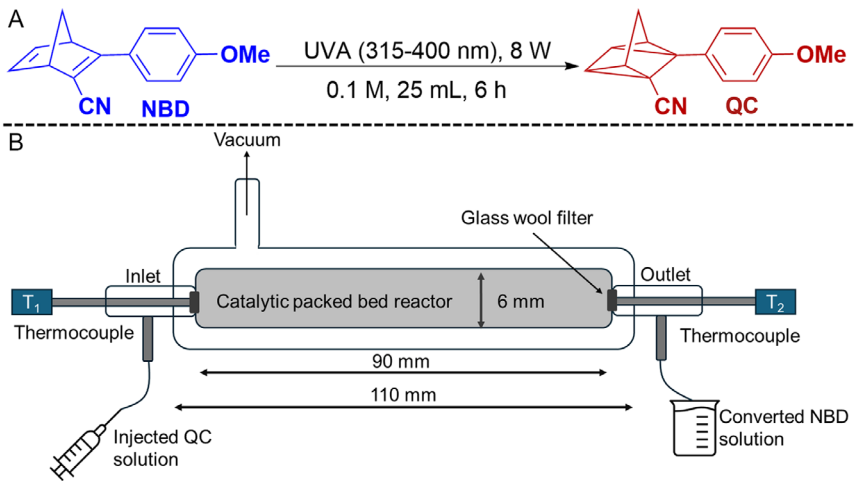

Figure 2. Photoisomerization procedure for a 0.10 M NBD solution dissolved in A) toluene and the B) flow setup for the catalytic back reaction of QC to NBD flowing through four differently sized packed beds in which sizes range from 250–315 µm, 315–500 µm, 500–710 µm, and 710–1000 µm.

Thus, four different catalyst were synthesized and characterized to verify variations in catalyst design. The catalysts were characterized using a range of structural, surface, spectroscopic, and thermal techniques including X-ray diffraction, nitrogen physisorption, pulse chemisorption, diffuse reflectance infrared Fourier-transform spectroscopy, and temperature-programmed reduction. (See in Section Characterization, Supporting Information) Structure–reactivity relationships of the heterogeneous catalysts were investigated both in batch and flow conditions. To report the site time yield for this catalytic reaction, pulse chemisorption was applied to determine the dispersion of active catalytic sites exposed to incoming QC reactant molecules inside the reactor. The turnover number (TON) of the catalyst is evaluated for this solid–liquid MOST reaction by conducting multiple flow reactions on the same catalyst packed bed. Complementary to the flow reactions, computational fluid dynamic (CFD) simulations applying lattice-Boltzmann methods were performed on two packed beds of different particle sizes to evaluate the deviations in hydrothermal behavior along the reactor bed and within the interstices of the porous network. Details at the pore scale are explored including the mixing dynamics when changing the particle size and the applied flow rate.

2. Results and Discussion

2.1. Synthesis and Characterization

To study the flow and thermal profiles of the MOST fluid in the packed-bed reactor, a set of four platinum on activated carbon catalysts were prepared of varying particle sizes. The raw materials and synthesis method remained identical for all four catalysts, in this way key properties including metal–support interaction, oxidation state of the metal, active site distribution, and pore structure vary minimally. A granular Norit RX3 Extra activated carbon was selected due to its large surface area, high pore volume, high abrasion resistance, and commercial availability. The activated carbon was ground down using a pestle and mortar, then different mesh sizes were used to sieve particles to a defined size range. The four distinctly sized catalysts were prepared by the conventional incipient wetness impregnation method using a 5 wt% ratio of platinum per catalyst and calcinated in a muffle furnace. Using this conventional impregnation method, metal loadings and active site distribution can vary over the carbon support, in which likely a significant proportion of active sites are embedded in the porous network taking an eggshell structure.[14] By changing the physical dimensions of the catalyst yet retaining similar chemical properties, the reaction differences become more dependent on mass transport limitations and reactor geometries. The textural properties of the sized catalysts were examined by physisorption using N_2 as a probe molecule at 77 K. In **Table 1**, the validation in the similarity of the physical structures of the sized catalysts was evaluated by analyzing their surface areas, pore volumes, and pore sizes.

Considering that the preparation of activated carbon is prone to batch-to-batch variability due to processing discrepancies and varying ash content, these sized catalysts vary minimally in pore structure noticing differences of ±10% in surface area. The location of the active sites when prepared by impregnation methods is predominantly concentrated on the surface of the support.

Table 1. Gas sorption data of sized Pt on activated carbon catalysts using a quantized liquid density-functional theory (QL-DFT) model. Physisorption data is crossreferenced against catalytic batch reactions recorded after 1 h. The concentration of converted NBD molecules is quantified.

Catalyst	Catalyst size [µm]	BET surface area [m^2 g])	Pore volume [cm^3 g]	Pore size [nm]
1	250-315	1411	0.662	9.5
2	315-500	1634	0.789	9.7
3	500-710	1502	0.716	9.8
4	710-1000	1423	0.691	9.9
Norit RX3 Extra	–	1370	0.620	9.0

© 2024 The Author(s). Advanced Energy and Sustainability Research published by Wiley-VCH GmbH

26999412, 2025, 1, Downloaded from https://onlinelibrary.wiley.com/doi/10.1002/aesr.202400230 by Chalmers University Of Technology, Wiley Online Library on [30/01/2025]. See the Terms and Conditions (https://onlinelibrary.wiley.com/terms-and-conditions) on Wiley Online Library for rules of use; OA articles are governed by the applicable Creative Commons License

Moreover, platinum nanoparticles have a high value in free surface energy; hence, clusters commonly form on the support. Thus, only a fraction of the deposited metal is exposed to the reagents flowing over them in the reactor. To calculate the turnover frequency value, the number of exposed active platinum sites dispersed on the sized catalysts was determined by pulse chemisorption using CO as a molecular titrant. In our case, we report a site time yield (STY) which can be defined as the number of norbornadiene (product) molecules made per catalytic site per unit time (residence time in the flow reactor).[15,16] Equation (1) was used to calculate dispersion %

$$\left(\left(D = nx\frac{\text{Vads}}{Vg}x\frac{m \times w}{M}x100\right)\right) \tag{1}$$

where n is the stoichiometry factor, V_{ads} is the volume adsorbed ($cm^3\,g^{-1}$), V_g is the molar volume of gas at STP ($22\,414\,cm^3\,mol^{-1}$), $m \times w$ is the molecular weight of metal, and M is % metal loading.

Generally, the catalysts exhibit a low dispersion of active sites confirmed by CO chemisorption (See in Table S4, Supporting Information). Plus, in conjunction with the powder X-ray diffraction results, the catalyst particles are of an amorphous nature and can be assumed to be of polyhedral deformed shapes.

2.2. Catalytic Performance of the QC-NBD Back Reaction in Batch Conditions

In the catalytic batch reactions, the catalyst particles are dispersed in the QC solution and under mechanical stirring, smaller particles are increasingly suspended within the solution. Three of the four catalysts follow a trend in which the smaller-sized catalysts are becoming faster as the reaction progressed (See in Figure S13, Supporting information). The exception was the largest-sized catalyst which performed fastest, although from visual inspection, the reaction began with only two larger grain-size catalyst particles and broke down into finer ones (See in Figure S14, Supporting information). As smaller particles are more homogeneously dispersed throughout the solution, the mass transfer distance of reagents to active sites becomes shorter, as shown in **Figure 3**,4.[17]

2.3. Flow Reactions

In a packed-bed reactor flow setup, the catalytic particles are in a stationary arrangement, far less prone to physical deactivation processes like attrition and agglomeration. An initial set of four flow experiments were performed for the sized catalysts in which the cylindrical reactor chamber was filled to a volume of $2.55\,cm^3$. 0.1 M solutions flowed through the reactor at a rate of $100\,mL\,h^{-1}$. A clear trend shown in **Table 2** is established in which the smaller-sized catalysts achieve 100% conversion of QC to NBD while larger catalysts convert minorly less NBD. It is noticeable that the packed-bed density for the smallest particle size range increases significantly, in which the interstitial voids between the catalyst particles are reduced.

Here, the 315–500 µm catalyst 2 produces the highest activity and heat release in flow conditions. The specific particle size range of the catalyst affects the size and homogeneity of the interstices, altering the catalytic conversion and subsequent heat release. Across the cross section of the packed bed, a region in which the particles are packed regularly is known as the "inviscid core" and the region between the wall and catalyst particles whereby voids are more nonuniform contributes to what is commonly referred to as "wall" effects. For smaller particle sizes, the interparticle spacing in the inviscid core of the reactor bed

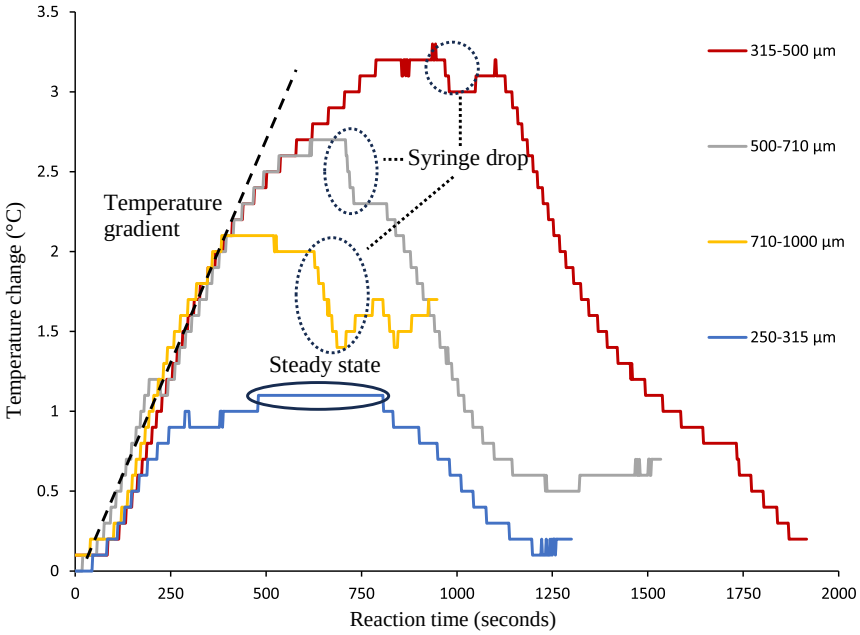

Figure 3. Thermal profiles over time of a 0.1 M 20/25 mL QC solution flowing through the reactor bed filled with different catalyst sizes at $100\,mL\,h^{-1}$. The temperature change (°C) between the two thermocouples with respect to room temperature is shown.

© 2024 The Author(s). Advanced Energy and Sustainability Research published by Wiley-VCH GmbH

26999412, 2025, 1, Downloaded from https://onlinelibrary.wiley.com/doi/10.1002/aesr.202400230 by Chalmers University Of Technology, Wiley Online Library on [30/01/2025]. See the Terms and Conditions (https://onlinelibrary.wiley.com/terms-and-conditions) on Wiley Online Library for rules of use; OA articles are governed by the applicable Creative Commons License

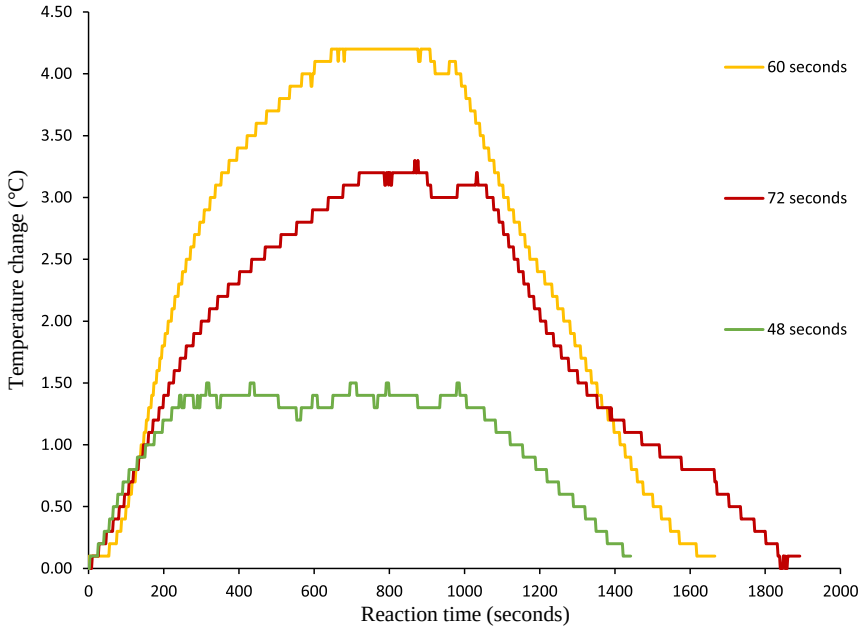

Figure 4. Heat release profiles of catalyst **2** (315–500 µm) when changing the residence times yet retaining the same flow rate of 100 mL h^{-1}.

Table 2. (Maximum thermal output and converted NBD measured from four flow reactions in packed bed reactors of different catalyst sizes. The converted NBD solution was measured by UV–vis spectroscopy. The activity was calculated from CO pulse chemisorption technique).

Catalyst	Thermal output [°C]	Packed-bed density [g cm^3]	Converted NBD [%]	Activity [mol g s^{-1}]
1	1.4	0.39	100	1.66×10^{-5}
2	3.2	0.28	100	3.56×10^{-5}
3	2.7	0.28	92	1.04×10^{-5}
4	2.1	0.29	86	1.37×10^{-5}

decreases, lowering the tortuosity of the flow path. Thus, higher packing ratios mean that the effective pore diffusion distance for QC reactants to reach active sites is reduced.

For catalyst 1, the thermal profile reaches 1.1 °C holding a "saturation regime" for *circa* 6.5 min much earlier than the other three catalysts. In the other thermal profiles, 20 mL of QC solution does not seem to be sufficient volume to achieve a stationary regime as a plateau is witnessed for 126 and 84 s for catalyst 4 and 3 respectively. Thus, for catalyst 2, a 25 mL of QC solution flows in which a stationary regime was attained at 3.2 °C for *circa* six minutes. Although, in some cases, a noticeable drop is observed due to a change in syringes to push through the remaining QC solution. For each thermal profile, the temperature gradient is constant until the saturation regime is reached. Considering the temperature gradient is dictated principally by the specific heat capacities and the heat transfer between the catalyst bed, the MOST fluid, the surrounding glass walls, and the temperature sensor, this factor validates the reproducibility of the reaction setup.[18,19]

Even though the two smaller-sized catalysts achieve 100% conversion to NBD, the thermal output differs significantly. This difference was attributed to the 38% increase in mass of the packed bed. The catalytic reaction occurs at active platinum sites, whereby a 5 wt% of platinum is present, its high thermal conductivity of 77.8 W m. K with respect to 0.60 W m^{-1}. K for activated carbon suggests heat may be conducted by these particles reducing heat transferred by the MOST fluid via convection. Even though the catalytic material has the same specific heat capacity, the additional mass of catalyst in the same volume means to reach a thermal equilibrium, more heat is absorbed. Indirect experimental proof is demonstrated by packing the reactor with solely carbon particles of different grain sizes and flowing toluene through the packed bed, the heat released from the adsorption enthalpic interaction between carbon and toluene varies negligibly per grain size (see Figure S18, Supporting information). Furthermore, considering the smaller surface area to volume ratio, the increased macroscopic pellet density of the bed and an "eggshell" catalyst structure whereby platinum crystallites are predominantly located at the surface, more contact points are created between crystallites, subsequently increasing thermal conductivity. Next, the best-performing catalyst 2 (315–500 µm) is chosen for the second set of flow reactions, in which the reactor is filled up to different volumes, by shortening the actual length of the catalyst packed bed which is shown in **Table 3**. The flow rate is kept constant for each flow reaction at 100 mL h^{-1} to obtain the conversion rate in percent as a function of the molecular residence time.

A residence time of 60 s proved to be sufficient to attain complete catalytic conversion to NBD, whereby shortening the contact time by 12 s causes a decrease in conversion of ≈50%. In these heat-release profiles stationary regimes were achieved, although interestingly the medium reactor volume reaches a higher heat release. Once again, using a greater mass of catalyst

© 2024 The Author(s). Advanced Energy and Sustainability Research published by Wiley-VCH GmbH

26999412, 2025, 1, Downloaded from https://onlinelibrary.wiley.com/doi/10.1002/aesr.202400230 by Chalmers University Of Technology, Wiley Online Library on [30/01/2025]. See the Terms and Conditions (https://onlinelibrary.wiley.com/terms-and-conditions) on Wiley Online Library for rules of use; OA articles are governed by the applicable Creative Commons License

Table 3. (Conversion percent and heat releases of catalyst 2 (315–500 μm) whereby molecular residence time is changed, using a constant flow rate of 100 mL h^{-1}. The reactions were carried out twice to confirm reproducibility of flow reaction conditions. The converted NBD solution was measured by UV–vis spectroscopy).

Reactor bed length [cm]	Packed bed density [g cm^{-3}]	Residence time [s]	Converted NBD % 1st exp/2nd exp	Thermal output [°C]
9	0.28	72	100/98	3.2/3.0
7.5	0.23	60	98/95	4.2/3.8
6	0.18	48	47/45	1.6/1.4

than actually required to reach 100% conversion, the overall thermal output is reduced. In these runs, the same particle size is used implying that the packing ratio impacts minorly on the maximum heat lift reached during the experiment. Aside from the higher packed bed density augmenting the overall specific heat capacity of the bed, an added factor can be that a supplementary residence time of 12 s results in some heat lost from the device to its surroundings.

Thereafter the effect of changing flow rates was analyzed for the catalytic heat release of the MOST fluid. The packed-bed mass and length were altered but the residence time of the reactants in the flow reactor was retained at 72 s. In this setup, the reactions are no longer dependent on chemical features like the residence time and temperature distribution along the reactor **Table 4**.

It is found that the chemical reaction does not follow a trend whereby the chemical conversion changes by ±6% over the three reactions likely due to minor deviations in the catalytic reactor volumes and the irradiated NBD solutions. As presumed, the heat release decreases sequentially by ≈0.5 °C when applying lower flow rates through the catalyst beds. Despite all these flow reactions likely taking a laminar flow profile, going to lower flow rates, the mixing and advection along the reactor decreases, wherein the viscous forces become more dominant than the inertial ones.[20]

Finally, the TON is a measure of catalyst lifetime, it is defined as the number of catalytic cycles a site can turnover until complete deactivation. To accurately witness deactivation of catalyst activity from a high activity level to inactive, the flow rate of reagents applied is much higher producing moderate conversions. At full conversion, only a minimum catalytic activity can be determined, because reagent availability limits conversion; the catalyst could actually be much more active.

Table 4. Heat release from catalyst 3 (500–710 μm) for scale-up wherein molecular residence time of quadricyclane solution in the catalytic reactor is constant at 72 s. The converted NBD solution was measured by UV–vis spectroscopy.

Reactor bed length [cm]	Packed bed density [g cm^{-3}]	Flow rate [mL h^{-1}]	Converted NBD [%]	Heat release [°C]
9	0.28	100	92	2.7
7.5	0.23	83	86	2.1
6	0.18	67	89	1.6

A minimum of five runs were performed across the same length catalyst bed of 7.5 cm, containing freshly produced catalyst. The flow rate utilized is 125 mL h^{-1} giving a residence time of 52.5 s.

First, by shortening the molecular residence time of QC with the catalyst, the converted NBD molecules recorded is reduced significantly to ≈60–70%. Over the five runs, a total drop of 4% in conversion occurs; thus, a sequential reduction in activity of ≈0.75% is assumed. The TON can be calculated from the integral of the changes in activity over time (see in Equation S(5), Supporting Information) The TON for catalyst 2 under exposure to QC reactants is relatively high, calculated as 31.28 h^{-1}. In addition, a material fatigue of the NBD-QC photoswitch has previously been asserted as 0.14% degradation per cycle over 43 photoirradiation and thermal cycles,[7] demonstrating the practical viability of a catalyst integrated MOST system.

2.4. Computational Fluid Dynamic (CFD) Simulations

In this section, the fluid-dynamic behavior of the reactor is investigated by means of CFD simulations, to elucidate the role of flow intensity in the mixing and conversion of reactants. Because the flow and mixing of the reactant solution is determined at the pore scale (the length of the pore interstices between individual catalyst particles), the mass and momentum equations are solved via the lattice Boltzmann method, a molecular-based model that allows pore-scale resolution of the transport dynamics.[21]

A solution is continuously injected into a segment of the tubular reactor, reconstructed in silico as a fixed packed bed with specified catalyst particle sizes of 533 and 800 μm is chosen for simulations, respectively. These two particle sizes are chosen as they correlate with the synthesized catalysts 3 and 4. A smaller catalyst size was not selected due to the computational demanding nature of the simulations, whereby this difference in size was deemed great enough to observe changes in hydrodynamic behavior. A first-order reaction is imposed at the fluid–catalyst interface. The two simulation snapshots shown in **Figure 5** refer to the two configurations which differ in particle size and flow rate (higher with smaller particle size), whereas the main characteristics of the flow are maintained equal by setting the same Reynolds (advective-to-viscous forces ratio **Figure 6**, $\mathrm{Re} = 0.6$), Peclet (advective-to-diffusive rates ratio, $\mathrm{Pe} = 290$), and Damköhler (reaction-to-longitudinal transport rates ratio, $\mathrm{Da} = 2$) numbers (see also table in Figure 5).

The observed discrepancies in flow behavior are thus expected to emerge due to spatial differences in geometrical features, such as the catalyst particle packing and interparticle pore distribution. It will be shown that this is indeed the case and that geometrically induced advective rates determine the efficiency of mixing. In Figure 5, elements of concentration, stretched by flow-sustained advection, are visibly forming inside the reactor's porous structure, particularly in the vicinity of the mean front position, whilst a more uniform distribution of concentration is observed in the configuration with smaller particles and higher flow rate (right panel). This kind of flow-induced deformation and mixing is typically observed at high Péclet numbers.[22] The overall dynamics of the system is characterized by three different characteristic time scales: the reaction time t_k determining mass transfer at

© 2024 The Author(s). Advanced Energy and Sustainability Research published by Wiley-VCH GmbH

26999412, 2025, 1, Downloaded from https://onlinelibrary.wiley.com/doi/10.1002/aesr.202400230 by Chalmers University Of Technology, Wiley Online Library on [30/01/2025]. See the Terms and Conditions (https://onlinelibrary.wiley.com/terms-and-conditions) on Wiley Online Library for rules of use; OA articles are governed by the applicable Creative Commons License

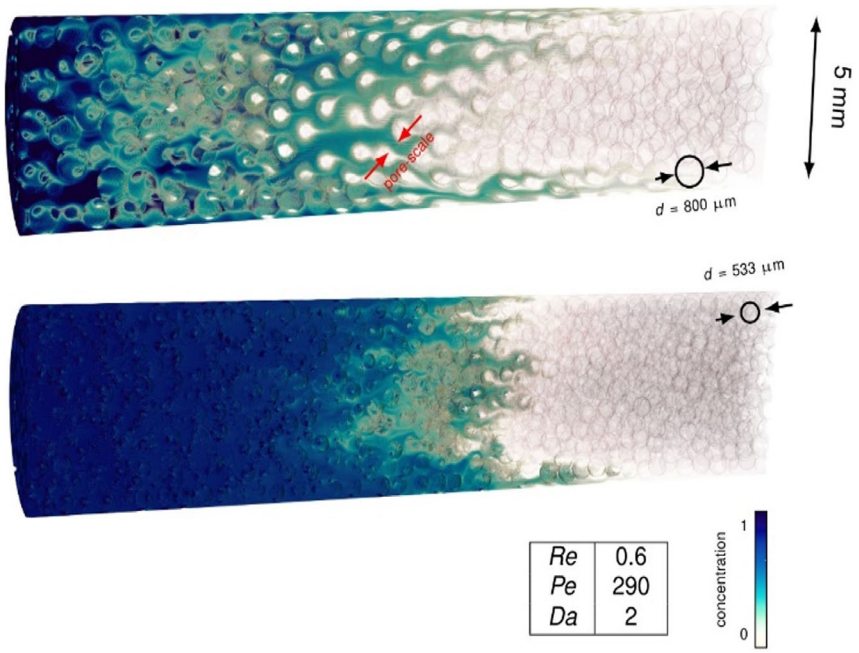

Figure 5. Snapshots of simulations of the continuous injection of a solution (high concentration in dark blue) within the porous catalyst reactor, with two different catalyst particle sizes.

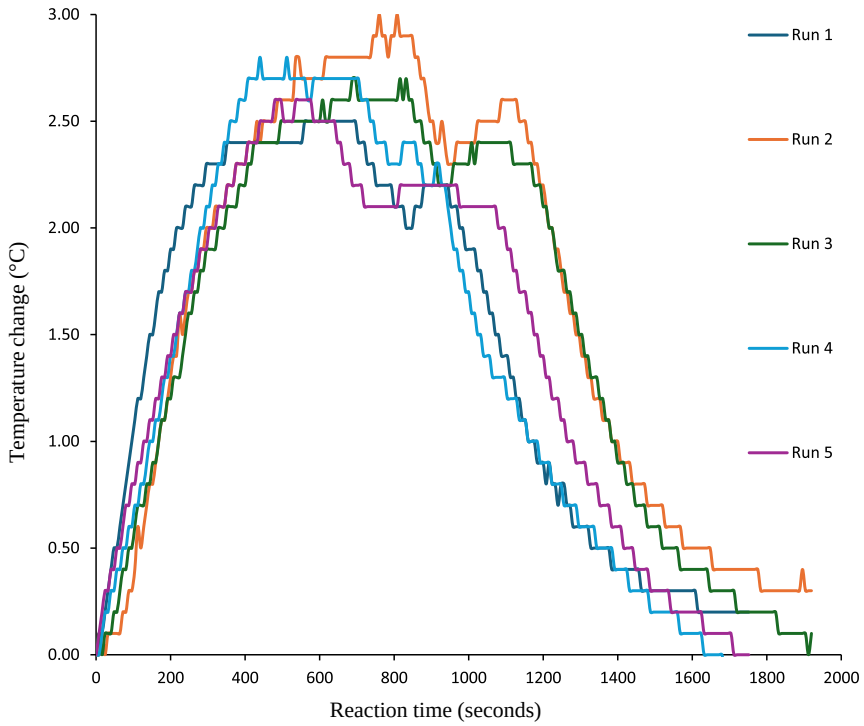

Figure 6. Heat release profiles from catalyst 2 (315–500 µm) whereby a 0.1 M QC solution is flowed through the reactor at a rate of 125 mL h^{-1} through a reactor volume of 0.23 cm^3 g^{-1}.

the fluid–catalyst particle interface, the molecular residence time in the reactor $t_r = L/U$, where L is the reactor length and U is the mean flow velocity, and the mixing time t_m. The latter is the characteristic time corresponding to the onset of overlapping between concentration elements; thus, it sets the onset of solute mixing. It is primarily a function of the pore scale advection rate

© 2024 The Author(s). Advanced Energy and Sustainability Research published by Wiley-VCH GmbH

26999412, 2025, 1, Downloaded from https://onlinelibrary.wiley.com/doi/10.1002/aesr.202400230 by Chalmers University Of Technology, Wiley Online Library on [30/01/2025]. See the Terms and Conditions (https://onlinelibrary.wiley.com/terms-and-conditions) on Wiley Online Library for rules of use; OA articles are governed by the applicable Creative Commons License

$t_m \approx d/U$ (and only weakly depending on the Péclet number),[23] where d is the hydrodynamic mixing length scale, that is, in this case, the catalyst particle size. The rapid onset of mixing is enhanced by high flow rates. A sketch of the mixing dynamics is presented in **Figure 7**, left panel (a): deformation of concentration elements along the flow direction (black arrow) initially compresses concentration elements along the transverse direction (red arrows); this compression steepens the transversal concentration gradients up to a point, the mixing time t_m, where transversal diffusion becomes dominant, and the concentration elements get diluted along the transversal direction (red arrows). Over a longer duration, the chemical reaction term, t_k, highlights the interfacial mass transfer-induced effects of the catalyst reaction, limiting concentration elements deformation, as a consequence of reducing the extent of mixing.

In Figure 7b, right panel, the time dependence of the mean-normalized variance $(\sigma_{cat}/\mu_{cat})^2$ of concentration at the fluid–catalyst interface in the vicinity of the solution front (see Figure 5) is reported. Its decay, which is a measure of mixing, is clearly determined by the mixing rate $1/t_m$, while its asymptotic values at long times depend on the reaction-to-mixing times ratio (thus neither on the Re, Pe, or Da numbers) via an inversely proportional relationship.

$$((\sigma^2{}_{cat}/\mu^2{}_{cat} = (t_k U/d)^{-\alpha})) \tag{2}$$

where $\alpha \approx ½$ is here observed (blue line, Figure 7), a signature of the dominant direction of mixing along the transverse direction. From this computational analysis it appears clear that reaction homogeneity is improved, and mass transport limitations are

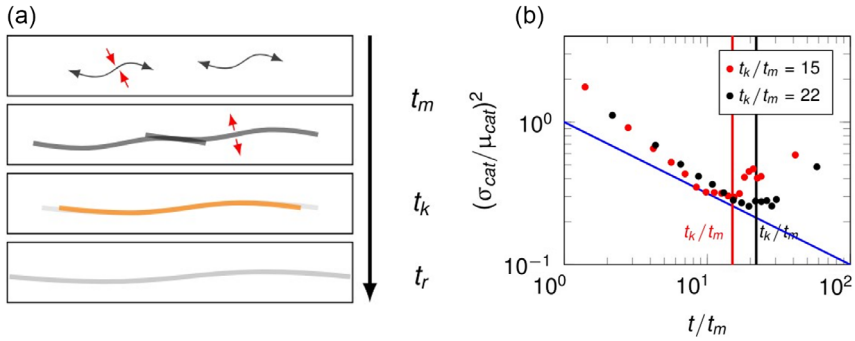

Figure 7. Left panel a): Schematic of mixing dynamics longitudinally stretched and successively diluted in the pore interstices along the reactor wherein t_m represents the mixing time, t_k represents the reaction time, and t_r represents the molecular residence time. Right panel b): concentration variance decay at the catalyst–electrolyte interface as a measure of dynamic mixing in the reactor.

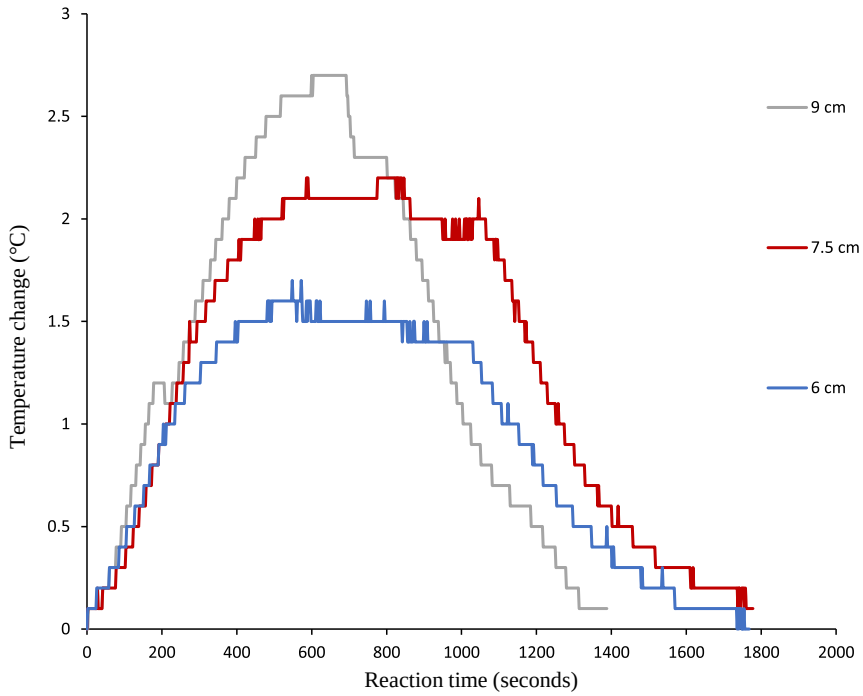

Figure 8. Heat release profiles from catalyst 3 (500–710 μm) retaining the same residence time but changing the flow rates and reactor volumes accordingly.

© 2024 The Author(s). Advanced Energy and Sustainability Research published by Wiley-VCH GmbH

26999412, 2025, 1, Downloaded from https://onlinelibrary.wiley.com/doi/10.1002/aesr.202400230 by Chalmers University Of Technology, Wiley Online Library on [30/01/2025]. See the Terms and Conditions (https://onlinelibrary.wiley.com/terms-and-conditions) on Wiley Online Library for rules of use; OA articles are governed by the applicable Creative Commons License

inhibited by either 1) small particle sizes or 2) high flow velocities, since both strategies lead to low-concentration variance at the catalyst surface. From an engineering perspective, both strategies come at the cost of a higher pressure drop, which scales as $\Delta P \propto (\mathrm{U\,L\,d}^{-2})$, by requiring either 1) a larger particle size d or 2) a longer reactor L that ensures $t_r = L/U > t_k$ for high flow velocities U. Nonetheless, the latter strategy may be preferable because it minimizes the risk of pore occlusions. Its effectiveness has been confirmed in the present experimental study (see **Figure 8**).

In this study, we found that the ideal particle size at *circa* 500 µm is marginally under one-tenth of the reactor diameter, resulting in the highest catalytic conversions and temperature changes. Despite the packing density differing negligibly when testing packed beds of larger particle sizes, discrepancies in the flow behavior are present. From CFD simulations, it was found that the flow profiles of packed beds with smaller particle sizes have a more homogenous concentration distribution across the reactor diameter whilst at larger particle sizes, the interparticle spacing of the particles induces concentrated portions of reactants to be dispersed along the reactor in a longitudinal fashion. The snapshots in Figure 5 depict a lower tortuosity in the flow profile supporting experimental results in which lower conversions were found for larger particles. Even if the molecular residence time in the reactor is the same, the overall diffusion distance of the QC reagents is reduced, in turn inhibiting mass transport to active catalytic sites. Combining both experimental and CFD simulations has imparted a wider insight into effectively scaling up heterogeneously catalyzed MOST reactions.

3. Conclusion

To conclude, the effects of changing the catalyst particle size and subsequent packing ratio in a specially designed double glass-walled reactor were studied experimentally and through fluid dynamic simulations. In general, the smaller particle sizes attained higher activities, plus a near-inverse parabolic flow profile in solution was generated resulting in a more homogeneous distribution of reactants across the reactor cross section. A high site time yield and TON were found up to 3.56×10^{-5} mol g^{-1}. s and 31.28 h^{-1}, respectively, allowing future prediction of parameters to employ when exposed to higher MOST concentrations. Moving toward larger-scale catalytic MOST reactions, real-life devices will likely not incorporate an ultrahigh-vacuum cell into the design. Thus, it will be necessary to adjust the molecular residence time to maximize the overall temperature output as the device will succumb to thermal losses. Positively, validated both computationally and experimentally, these thermal losses can be mitigated by increasing flow rates, enhancing the advective transport of the MOST fluid along the reactor. Furthermore, it was found that extra, unnecessary packing of catalyst particles can reduce the overall thermal output from the energy dense QC isomer. Future research should be focused on maximizing the heat release from MOST solutions by testing catalysts with lower metal loadings or different active sites to platinum which have lower thermal conductivities.

4. Experimental Section

Synthesis of Sized Catalysts: The Pt/C-supported (nominal 5.0 ± 0.5 wt% metal) activated carbon catalyst was synthesized by the conventional impregnation method (i.e., incipient wetness method).[24] A Norit RX Extra 3 mm activated carbon was washed with deionized water and dried overnight at 120 °C in a Nabertherm muffle oven. Here, 950 mg of activated carbon and 5 wt% (81.4 mg) of platinum nitrate precursor metal was added for each catalyst. The pore volume of the Norit RX3 Extra activated carbon was 620 µL g^{-1}; thus, to fill the exact pore volume, each metal precursor was dissolved in 589 µL of ethanol. The precursor solution was added dropwise using a syringe pump at a rate of 10 µL min^{-1} to the carbon support. The sample was mixed thoroughly prior to placing it in the muffle oven. First, a ramp in temperature was applied from 25–120 °C at 60 °C h^{-1}, the temperature was held at 120 °C for 2 h, next a ramp in temperature from 120–300 °C at 60 °C h^{-1} was done, and finally the samples were calcined at 300 °C for 12 h. The sample was cooled to room temperature and stored in an air-tight vial prior to use.

Characterization: Powder X-ray diffraction patterns were recorded using a Rigaku Diffractometer using Cu Kα radiation ($\lambda = 1.54$ Å). From data collected during nitrogen adsorption–desorption measurements at 77 K on an Anton Paar QuadraSorb instrument, the specific area was calculated using the Brunauer–Emmett–Teller (BET) method, and the pore volume and the pore size distribution were calculated using a quantized solid density functional theory model. The active site dispersion was measured using pulse chemisorption with CO as the molecular titrant. Temperature-programmed reduction was performed using an AMI-300 instrument. Diffuse reflectance Fourier-transform infrared spectra were recorded using a PerkinElmer Lambda Spectrum Two Fourier-transform infrared spectroscopy instrument. Metal loadings were measured using a PinAAcle 500 Flame Atomic Absorption Spectrometer instrument after the samples were digested in acid. NMR characterization of the NBD and QC pair was accomplished using a Bruker 400 MHz spectrometer.

Catalytic Activity Measurements: The catalytic batch reactions were conducted whereby the catalyst particles were in suspension and stirred continuously at a rate of 500 rpm. 10 mL solution of NBD and 1 mg mL^{-1} in toluene was irradiated using an 8 W LuzChem photoreactor with a UVA (315–400 nm) light source for ≈1 h until less than 2% NBD remained in the solution (determined by UV–vis spectroscopy). A 10 wt% of catalyst relative to NBD was added to the QC solution, wherein the reaction was monitored at specific time intervals using UV–vis spectroscopy. All UV–vis measurements were conducted using a Shimadzu UV–vis–NIR spectrophotometer. The first set of flow reactions were performed using 20 mL of 0.10 M solutions of NBD and then 25 mL of 0.10 M solutions of NBD, in both cases solutions were irradiated using a UVA (315–400 nm) light source for ≈6 h under gentle stirring at 300 rpm. The NBD conversion was monitored by UV–vis spectroscopy until less than 5% NBD remained in the solution. The packed-bed reactor was filled with a catalyst of a specific particle size range to a reactor volume of 2.55 cm^3 using glass wool at both ends to keep the particles in a fixed position and to collect the converted NBD solution. The ingoing QC solution and outgoing NBD solution flowed through the perpendicular joints of the T-shaped connector. A pair of Pt-100 thermocouples were placed in parallel with the reactor at both inlet and outlet ends, wherein a Dostmann P300 thermometer recorded the reaction's temperature change. (See Figure S16 and S17, Supporting information). The flow experiment was conducted in three steps: first, pure toluene flowed through the catalyst bed to avoid a bias in the generated temperature profile due to the enthalpic adsorption of toluene on the catalyst surface. Second, using a syringe pump, the QC solution was injected through the packed-bed reactor at a rate of 100 mL h^{-1}. Third, another 25 mL solution of toluene was passed through the reactor to push the remaining QC-NBD solution through the reactor. Note, a change in syringes meant the flow of QC solution was shortly interrupted, resulting in a small temperature drop after 600 s.

© 2024 The Author(s). Advanced Energy and Sustainability Research published by Wiley-VCH GmbH

26999412, 2025, 1, Downloaded from https://onlinelibrary.wiley.com/doi/10.1002/aesr.202400230 by Chalmers University Of Technology, Wiley Online Library on [30/01/2025]. See the Terms and Conditions (https://onlinelibrary.wiley.com/terms-and-conditions) on Wiley Online Library for rules of use; OA articles are governed by the applicable Creative Commons License

Supporting Information

Supporting Information is available from the Wiley Online Library or from the author.

Acknowledgements

The authors thank the European Union's H2020 research and innovation program under grant agreement no. 951801 (MOST H2020-EIC-FETPROACT-2019-951801). D. S. and I. F. A. acknowledge the MICIU/AEI/https://doi.org/10.13039/501100011033 and the European Union (NextGenerationEU/PRTR) for funding the project TED 2021-131896B-I00. I.F.-A. thanks the "Ministerio de Ciencia e Innovación" for the Juan de la Cierva-Incorporation scholarship (IJC2020-045 125-I). The computations were enabled by resources provided by the National Academic Infrastructure for Supercomputing in Sweden (NAISS), partially funded by the Swedish Research Council through grant agreement no. 2022-06725, Fraunhofer ISE, Philipp Hügenell (nitrogen physisorption) Universidad de la Rioja, Felix Gallarta (atomic absorption spectroscopy).

Conflict of Interest

The authors declare no conflict of interest.

Author Contributions

Lucien Magson: Investigation (lead); Writing—original draft (lead). **Dario Maggiolo**: Investigation (supporting); Writing—original draft (supporting). **Angela Sasic Kalagasidis**: Funding acquisition (supporting); Writing—review and editing (supporting). **Stefan Henninger**: Funding acquisition (supporting). **Gunther Munz**: Investigation (supporting); Writing—review and editing (supporting). **Markus Knäbbeler-Buß**: Data curation (supporting); Formal analysis (supporting); Investigation (supporting); Writing—original draft (supporting); Writing—review and editing (supporting). **Helen Hölzel**: Writing—review and editing (supporting). **Kasper Moth-Poulsen**: Funding acquisition (supporting); Writing—review and editing (supporting). **Ignacio Funes-Ardoiz**: Conceptualization (supporting); Writing—review and editing (supporting). **Diego Sampedro**: Conceptualization (supporting); Funding acquisition (lead); Writing—review and editing (supporting).

Data Availability Statement

The data that support the findings of this study are available in the supplementary material of this article.

Keywords

catalysts, energy storages, flow reactors, heat, rechargeable

Received: July 30, 2024
Revised: September 4, 2024
Published online: September 19, 2024

[1] Agency, *I.E. World Energy Outlook 2022*, IEA Publications, Paris **2022**.
[2] D. Wang, Y. Chen, M. Jarin, X. Xie, *npj Clean Water* **2022**, *5*, 36.
[3] Agency, *I.E. World Energy Outlook 2023*, IEA Publications, Paris **2023**.
[4] A. Dreos, K. Borjesson, Z. Wang, A. Roffey, Z. Norwood, D. Kushnir, K. Moth-Poulsen, *Energy Environ. Sci.* **2017**, *10*, 728.
[5] X. Xu, Y. Xing, Y. Yin, W. Fang, B. Wu, P. Bei, J. Feng, H. Yu, G. Wang, W.-Y. Li, *Chem. Eng. J* **2023**, *466*, 143175.
[6] M. Cazals, E. Bedard, M. Doberva, S. Faucher, M. Prevost, *Microorganisms* **2022**, *10*, 443.
[7] Z. Wang, A. Roffey, R. Losantos, A. Lennartson, M. Jevric, A. U. Petersen, M. Quant, A. Dreos, X. Wen, D. Sampedro, K. Borjesson, K. Moth-Poulsen, *Energy Environ. Sci.* **2019**, *12*, 187.
[8] M. Manso, A. U. Petersen, Z. Wang, P. Erhart, M. B. Nielsen, K. Moth-Poulsen, *Nat. Commun.* **2018**, *9*, 1945.
[9] J. Martyn, A. U. Petersen, M. Manso, S. S. Kumar, Z. Wang, A. Dreos, C. Sumby, M. B. Nielsen, K. Borjesson, P. Erhart, K. Moth-Poulsen, *Eur. J. Org. Chem.* **2018**, *24*, 12767.
[10] V. Gray, A. Lennartson, P. Ratanalert, K. Borjesson, K. Moth-Poulsen, *Chem. Commun.* **2014**, *50*, 5330.
[11] J. Orrego-Hernandez, H. Hölzel, M. Quant, Z. Wang, K. Moth-Poulsen, *J. Org. Chem.* **2021**, *2021*, 5337.
[12] N. Baggi, H. Hölzel, H. Schomaker, K. Moreno, K. Moth-Poulsen, *ChemSusChem* **2023**, *17*, e202301184.
[13] R. Baetens, B. P. Jelle, J. V. Thue, M. J. Tenpierik, S. Grynning, S. Uvslokk, A. Gustavsen, *Energy Build.* **2010**, *42*, 147.
[14] A. K. K. Vikla, I. Simakova, Y. Demidova, E. G. Keim, L. Calvo, M. A. Gilarranz, S. He, K. Seshan, *Appl. Catal., A* **2021**, *610*, 117963.
[15] P. B. Weisz, *CHEMTECH* **1992**, *22*, 424.
[16] S. Kozuch, J. M. L. Martin, *ACS Catal.* **2012**, *2*, 2787.
[17] M. J. E. da Silva, L. Lefferts, J. A. F. Albanese, *J. Catal.* **2021**, *402*, 114.
[18] S. R. Sunderesan, N. N. Clark, *Int. J. Multiphase Flow* **1995**, *21*, 1003.
[19] X. Yao, Y. Zhang, C. Lu, X. Han, *AIChE. J.* **2015**, *61*, 68.
[20] T. Suekane, Y. Yokouch, S. Hirai, *AIChE J.* **2003**, *49*, 10.
[21] D. Maggiolo, D. O. Modin, A. S. Kalagasidis, *Phys. Rev. Fluids* **2023**, *8*, 024502.
[22] M. Dentz, J. J. Hidalgo, D. Lester, *Transp. Porous. Media* **2023**, *146*, 5.
[23] T. Le Borgne, M. Dentz, E. Villermaux, *J. Fluid Mech.* **2015**, *770*, 458.
[24] P. Munnik, P. E. de Jongh, K. P. de Jong, *Chem. Rev.* **2015**, *115*, 6687.

© 2024 The Author(s). Advanced Energy and Sustainability Research published by Wiley-VCH GmbH

26999412, 2025, 1, Downloaded from https://onlinelibrary.wiley.com/doi/10.1002/aesr.202400230 by Chalmers University Of Technology, Wiley Online Library on [30/01/2025]. See the Terms and Conditions (https://onlinelibrary.wiley.com/terms-and-conditions) on Wiley Online Library for rules of use; OA articles are governed by the applicable Creative Commons License